

Contrasting interactions of urban heat islands with dry and moist heat waves and their implications for urban heat stress

Dong-Hwi Kim^a, Kyeongjoo Park^a, Jong-Jin Baik^{a,*}, Han-Gyul Jin^{b,c,**}, Beom-Soon Han^d

^a School of Earth and Environmental Sciences, Seoul National University, Seoul 08826, South Korea

^b Department of Atmospheric Sciences, Pusan National University, Busan 46241, South Korea

^c Institute for Future Earth, Pusan National University, Busan 46241, South Korea

^d Department of Environmental Engineering, Inha University, Incheon 22212, South Korea

ARTICLE INFO

Keywords:

Urban heat island
Dry heat wave
Moist heat wave
Synergistic interaction
Heat stress

ABSTRACT

The synergistic interactions between urban heat islands (UHIs) and heat waves are of great concern due to their adverse impacts on urban residents and scientific interest. Here, we examine the interactions of UHIs with two types of heat waves, dry heat waves (DHW) and moist heat waves (MHW). For this, Daegu, a large city in South Korea, is selected and observational and reanalysis data from 2001 to 2022 are analyzed. DHW (MHW) is defined as the heat waves with daily mean relative humidity lower (higher) than its 10th (90th) percentile. The mean nighttime UHI intensity calculated using daily minimum 2-m temperatures is stronger under DHW by 1.07 °C and weaker under MHW by 0.24 °C than under non-heat waves. This indicates synergistic interactions between UHIs and DHW, but negative interactions between UHIs and MHW. Evaluation of four thermal discomfort indices shows that the prominent nighttime synergistic UHI-heat wave interactions can result in similar or even greater nighttime heat stress under DHW compared to MHW for urban residents, despite lower humidity. This study highlights the necessity of considering heat wave characteristics and the consequent UHI-heat wave interactions in assessing and managing urban heat-related risks.

1. Introduction

The urban heat island (UHI), a phenomenon that the near-surface air temperature in the urban area is higher than that in its surrounding rural area, has received much attention. The UHI occurs mainly due to differences in surface characteristics between urban and rural areas and it can increase heat stress and pose health risks (Oke, 1982; Tan et al., 2010). Many studies have shown that UHIs synergistically interact with heat waves (Tan et al., 2010; Li and Bou-Zeid, 2013; Founda et al., 2015; Li et al., 2015; Founda and Santamouris, 2017; Zhao et al., 2018; Jiang et al., 2019; Rogers et al., 2019; An et al., 2020; Nagarame et al., 2020; Zong et al., 2021; Park et al., 2023). Founda and Santamouris (2017) showed that in Athens, Greece, the daytime UHI intensity is stronger by 1–3.5 °C under heat waves than under non-heat waves. Zong et al. (2021) reported the synergistic interaction in Beijing, China, with the increase in hourly UHI intensity under heat waves reaching up to 1.77 °C. Park et al. (2023) revealed that in Seoul, South Korea, the UHI

* Corresponding author.

** Corresponding author at: Department of Atmospheric Sciences, Pusan National University, Busan 46241, South Korea.

E-mail addresses: jjbaik@snu.ac.kr (J.-J. Baik), hgjin@pusan.ac.kr (H.-G. Jin).

<https://doi.org/10.1016/j.uclim.2024.102050>

Received 11 April 2024; Received in revised form 11 June 2024; Accepted 30 June 2024

Available online 4 July 2024

2212-0955/© 2024 The Authors. Published by Elsevier B.V. This is an open access article under the CC BY license (<http://creativecommons.org/licenses/by/4.0/>).

intensity, which is calculated using daily minimum 2-m temperatures, is 0.53 °C stronger under heat waves than under non-heat waves. Zhao et al. (2018) reported that in 14 cities located in northeastern U.S., both daytime and nighttime UHI intensities overall increase under heat waves by 0.2 and 0.7 °C, respectively, compared to non-heat waves. Rogers et al. (2019) analyzed UHI intensities observed in southern Australian cities and showed that the nighttime UHI intensities in Melbourne and Adelaide are stronger under heat waves than under non-heat waves by up to 1.4 and 1.2 °C, respectively. These studies indicate different degrees of the synergistic interactions depending on many factors such as the geographical locations of cities and the time of day. The synergistic interactions between UHIs and heat waves can exacerbate heat stress and further increase health risks (Li and Bou-Zeid, 2013; Zhao et al., 2018; He et al., 2021). On the other hand, it was also revealed that UHIs do not significantly interact or negatively interact with heat waves in several cities including Perth, Australia, Singapore, Singapore, and Dijon, France (Rogers et al., 2019; Chew et al., 2021; Richard et al., 2021).

Based on the degree of humidity, heat waves can be classified into dry heat waves (DHW) and moist (or humid) heat waves (MHW). There have been studies on the circulation patterns, characteristics, and/or dynamics of DHW and MHW (An and Zuo, 2021; Ha et al., 2022; Luo et al., 2022; Li et al., 2023). Luo et al. (2022) defined DHW (MHW) as three or more successive days when the dry-bulb (wet-bulb) temperature exceeds its 90th percentile and the wet-bulb (dry-bulb) temperature does not exceed its 90th percentile. They showed that over Southern China, DHW (MHW) is associated with more northward (southward) shift of the western North Pacific subtropical high (WNPSH) and South Asian high. Ha et al. (2022) defined heat waves with relative humidity below 33% (above 66%) as DHW (MHW), and revealed that over East Asia, the anticyclonic circulation strengthens after the onset of DHW, while the locally generated anticyclonic anomalies trigger MHW. For UHIs, DHW and MHW provide different background states, and the difference in background state can result in different UHI-heat wave interactions. However, previous studies have not focused on how the UHI-heat wave interaction is influenced by various background states. Only a study, conducted by Park et al. (2023), examined this aspect and showed that the UHI-heat wave interaction in Seoul significantly varies with synoptic characteristics of heat waves. In this study, we examine for the first time whether the interactions between UHIs and DHW are contrasted with those between UHIs and MHW.

Various thermal discomfort indices can be used to assess urban heat stress under heat waves. Raymond et al. (2017) examined extremes of wet-bulb temperature in the United States and showed that changes in specific humidity play more important roles than changes in temperature in controlling heat stress generally. Using the heat stress index, Chen et al. (2019) studied global heat wave hazards and showed that when the humidity effect is not considered, the number of heat waves per year is underestimated by about 40–140 days in the humid and warm tropics during 2076–2095 under the Representative Concentration Pathway 4.5 (RCP 4.5) scenario. These studies point out the importance of humidity effect in assessing heat stress under heat waves. In this study, we also examine how UHI-DHW interactions and UHI-MHW interactions differently influence heat stress using various thermal discomfort indices. Daegu, South Korea, is chosen for this study. Daegu is one of the most populated cities in South Korea with a population of 2.4 million (<https://kosis.kr>) and exhibits pronounced UHIs (Park et al., 2013). Furthermore, Daegu experiences the strongest heat wave intensity and is the most vulnerable to health risks of heat waves among major cities of South Korea (Son et al., 2012), which necessitates the examination of UHI-heat wave interactions.

2. Data and methods

This study uses meteorological and reanalysis data for the period of 2001–2022. July and August are considered because in South Korea, most heat waves have occurred in those months (Baik et al., 2022). Daegu is located in the southeastern part of the Korean Peninsula (Fig. 1a and b). Daegu belongs to the humid subtropical climate (Cwa) according to the Köppen-Geiger climate classification

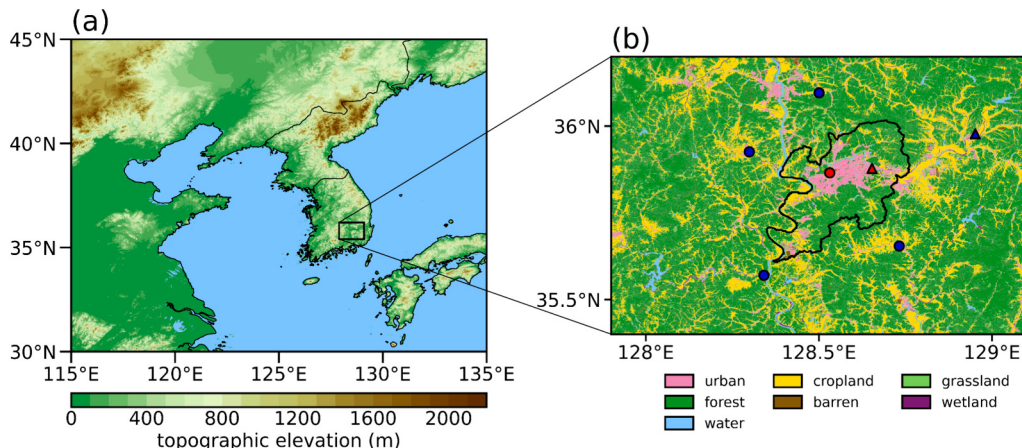


Fig. 1. (a) Map of South Korea and surrounding regions with topographic elevation. The black rectangle indicates Daegu and its surrounding areas. (b) Locations of automated synoptic observing systems (triangles) and automatic weather stations (circles). The red (blue) colour indicates the urban (rural) stations. The black solid line and colour shade indicate the administrative boundary of Daegu and the land use in 2022. (For interpretation of the references to colour in this figure legend, the reader is referred to the web version of this article.)

(Park et al., 2019). Among the seven major cities of South Korea (Seoul, Busan, Incheon, Daegu, Daejeon, Gwangju, and Ulsan), Daegu experiences the highest climatological mean air temperature (26.3 °C for 1991–2020) during July and August (<https://data.kma.go.kr>). The administrative boundary of Daegu and the locations of the weather stations whose data are used in this study together with the land use are shown in Fig. 1b. All these weather stations are operated by the Korean Meteorological Administration (<https://data.kma.go.kr>). One automated synoptic observing system (ASOS) and one automatic weather station (AWS) inside Daegu are selected as representative urban stations, and one ASOS and four AWSs around Daegu are selected as representative rural stations. The urban stations are mainly surrounded by residential and industrial areas, while the rural stations are mainly surrounded by agricultural land and forest. According to the land use data in 2022 produced by the Korea Ministry of Environment (<https://egis.me.go.kr>), the urban land use fraction averaged over the 1-km² circles surrounding the urban (rural) stations is 0.59 (0.16). The difference between elevation averaged over the urban stations and that averaged over the rural stations is 4 m. The data used are the hourly 2-m temperature, hourly 10-m wind speed, hourly dew-point temperature, hourly relative humidity, hourly cloud fraction (in tenth), daily maximum 2-m temperature (T_{\max}), daily minimum 2-m temperature (T_{\min}), and daily precipitation amount data. Note that the dew-point temperature, relative humidity, and cloud fraction data are available only for the ASOSs.

To examine large-scale circulation patterns and soil water, the fifth-generation European Centre for Medium-range Weather Forecasts reanalysis (ERA5) data (Hersbach et al., 2020) are used: 200- and 500-hPa geopotential heights, 200-, 500-, and 850-hPa zonal and meridional wind velocities, 850-hPa specific humidity, and volumetric soil water in the 0–7 cm soil layer. The temporal and horizontal resolutions of the ERA5 data are 1 h and 0.25° × 0.25°, respectively. The volumetric soil water is averaged over the 35.50–36.25°N and 128.25–129.00°E area.

The UHI-heat wave interaction is quantified as the difference in UHI intensity between heat waves and non-heat waves (Li and Bou-Zeid, 2013; Zhao et al., 2018). Following Park et al. (2023), $\text{UHII}_{T_{\min}}$ ($\text{UHII}_{T_{\max}}$) is defined as the daily minimum 2-m temperature T_{\min} (daily maximum 2-m temperature T_{\max}) averaged over the urban stations minus that averaged over the rural stations. A heat wave is defined as a phenomenon with a period of successive days when T_{\max} averaged over all stations is higher than 33 °C (Park et al., 2023). Using this definition, the total number of heat wave days during the study period is 439. In this study, the UHI-heat wave interactions under two types of heat waves, DHW and MHW, are examined. Here, we define DHW (MHW) as the heat waves when the daily mean relative humidity averaged over all stations is lower (higher) than its 10th (90th) percentile. These relative definitions are useful in examining varying UHI-heat wave interactions that Daegu actually experiences.

To study differences in meteorological and soil water conditions between DHW and MHW, the daily mean 10-m wind speed, daily mean relative humidity, and daily mean cloud fraction averaged over all stations and the daily mean volumetric soil water are analyzed. In calculating the daily mean value of any meteorological variable, the data from stations with above-20% missing data are excluded. Also, for each day, the data from stations with the daily precipitation amount larger than 0.1 mm are excluded from the analysis (Jiang et al., 2019; Park et al., 2023). This leaves 39 DHW days and 35 MHW days to be analyzed in this study.

To investigate associations between the UHI-heat wave interaction and urban heat stress, four thermal discomfort indices are adopted. These are the Humidex (Rana et al., 2013), wet-bulb temperature (T_w) (Stull, 2011), discomfort index (DI) (Epstein and Moran, 2006), and heat index (HI) (Blazejczyk et al., 2012) which are, respectively, expressed as follows:

$$\text{Humidex} = T + \frac{5}{9}(e - 10) \quad (1)$$

$$T_w = T \times \text{atan}\left(0.1520 \times (RH + 8.3137)^{1/2}\right) + \text{atan}(T + RH) \\ - \text{atan}(RH - 1.676) + 0.0039 \times RH^{2/3} \times \text{atan}(0.0231 \times RH) \\ - 4.6860 \quad (2)$$

$$DI = 0.5(T_w + T) \quad (3)$$

$$HI = \begin{cases} 0.2778 \times (1.8000 \times T + 29 + 2.1600 \times (T - 20) + 0.0940 \times RH) & (HI \leq 26.7^\circ\text{C}) \\ -8.7847 + 1.6114 \times T + 2.3385 \times RH \\ -0.1461 \times T \times RH - 1.2308 \times 10^{-2} \times T^2 - 1.6425 \times 10^{-2} \times RH^2 \\ + 2.2117 \times 10^{-3} \times T^2 \times RH + 7.2546 \times 10^{-4} \times T \times RH^2 & (HI > 26.7^\circ\text{C}) \\ -3.5820 \times 10^{-6} \times T^2 \times RH^2 \end{cases} \quad (4)$$

Here, Eqs. (1)–(4) are empirically obtained using the values of air temperature (T , °C), vapor pressure (e , hPa), relative humidity (RH, %), and/or T_w (°C). For example, for an air temperature of 30.1 °C, the value 30.1 is used. The Humidex and DI are unitless, and T_w and HI are in °C. In the calculation of HI, one of the two formulas is used depending on whether HI exceeds 26.7 °C (80.0 °F) or not, and additional adjustments are applied for certain ranges of temperature and relative humidity, which are described in detail in the National Oceanic and Atmospheric Administration website (<https://www.wpc.ncep.noaa.gov>). All these indices consider both temperature and humidity to quantify thermal discomfort perceived by human bodies. In calculating each index, T is averaged over the urban stations and RH and e at the urban ASOS (Fig. 1b) are used.

3. Results and discussion

3.1. Urban heat islands under heat waves

First, as was done in Park et al. (2023), the composite fields of 200- and 500-hPa geopotential heights and wind vectors are analyzed to examine large-scale circulation patterns associated with heat waves (HW) and non-heat waves (nonHW) (Fig. 2). In this figure, the isolines of 12,480-m geopotential height at the 200-hPa level and 5880-m geopotential height at the 500-hPa level are drawn, which are generally considered to represent the boundaries of the Tibetan high and WNPSH, respectively. As seen in the composite fields, the Tibetan high and WNPSH are typical summertime large-scale features observed in this region. Under HW, both the Tibetan high and WNPSH further expand toward the Korean Peninsula. At the 200-hPa level, the region of positive geopotential height differences, which covers the Korean Peninsula, is elongated in the east-west direction (Fig. 2c) and the wind difference is anticyclonic over the Korean Peninsula and its nearby regions (Fig. 2c). These features are also observed at the 500-hPa level (Fig. 2f). This kind of barotropic structure with the positive geopotential height differences facilitates subsidence and subsidence-induced adiabatic heating, contributing to the intensification and prolonged duration of heat waves over the Korean Peninsula (Lee and Lee, 2016; Xu et al., 2019; Lee et al., 2020).

Next, meteorological and soil water conditions under HW and nonHW are analyzed. The daily maximum 2-m temperature is 35.1 °C under HW and 30.3 °C under nonHW, the difference being as large as 4.8 °C. The daily mean relative humidity, daily mean cloud fraction, and volumetric soil water under HW (66.0%, 4.13, and 0.27 m³ m⁻³, respectively) are lower than those under nonHW (70.9%, 6.48, and 0.33 m³ m⁻³, respectively), confirming that heat wave days exhibit drier and clearer weather and less soil water than non-heat wave days. The differences in individual variables between HW and nonHW are statistically significant at the 95% confidence level. Hereafter, all statistical significance tests are made at the 95% confidence level.

The diurnal variations of UHI intensities under HW and nonHW are presented in Fig. 3. For both HW and nonHW, the UHI intensity is stronger in the nighttime than in the daytime, consistent with previous studies (Li et al., 2015; An et al., 2020; Park et al., 2023). The difference in UHI intensity between HW and nonHW is larger in the nighttime than in the daytime. $UHII_{Tmin}$ under HW is 1.91 °C and $UHII_{Tmin}$ under nonHW is 1.51 °C, and their difference is statistically significant. On the other hand, $UHII_{Tmax}$ under HW is 0.30 °C and $UHII_{Tmax}$ under nonHW is 0.30 °C, and their difference is statistically insignificant. We find that a clear synergistic effect is evident in

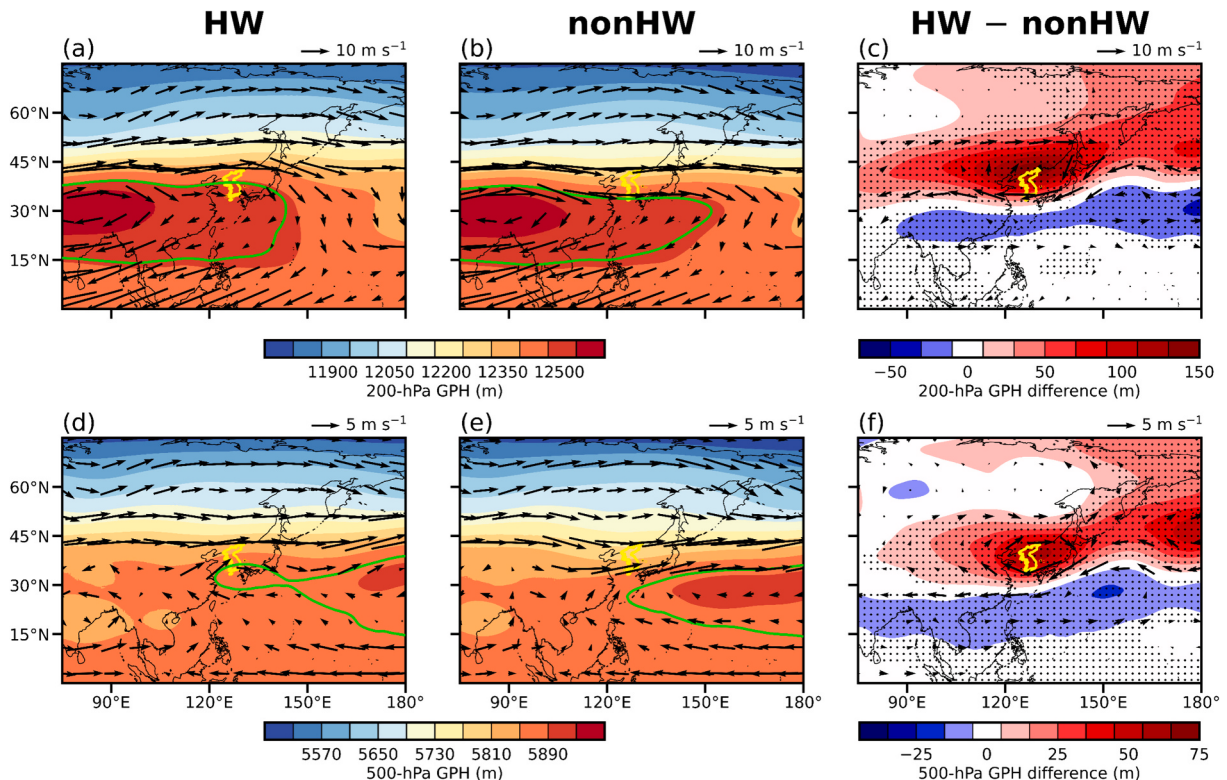


Fig. 2. Composite fields of geopotential heights (shaded) and horizontal wind vectors at the (a, b) 200-hPa level and (d, e) 500-hPa level under (a, d) HW and (b, e) nonHW and (c, f) their respective differences. The green contour lines in (a, b) and (d, e) indicate the boundaries of the Tibetan high (12,480 m) and western North Pacific subtropical high (WNPSH) (5880 m), respectively. The yellow solid line denotes the border of the Korean Peninsula. The dotted areas indicate that the difference is statistically significant at the 95% confidence level. (For interpretation of the references to colour in this figure legend, the reader is referred to the web version of this article.)

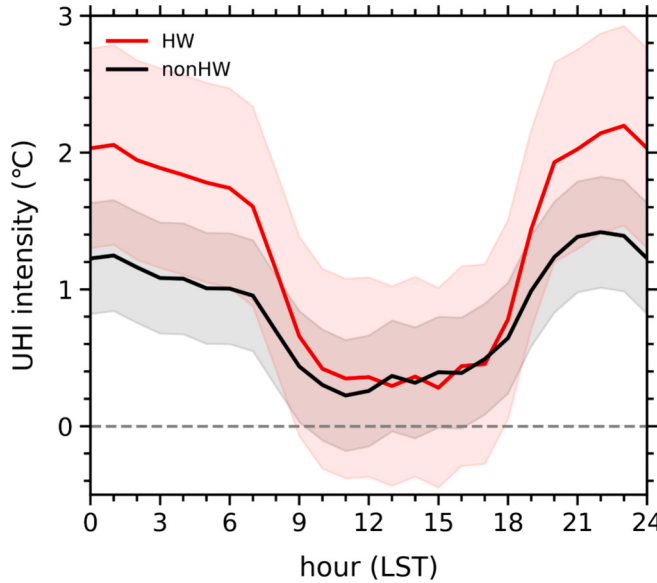


Fig. 3. Diurnal variations of urban heat island intensities under HW (red solid line) and nonHW (black solid line). The red and gray shaded areas denote one standard deviations of urban heat island intensities under HW and nonHW, respectively. (For interpretation of the references to colour in this figure legend, the reader is referred to the web version of this article.)

the nighttime, while there is no distinct synergistic effect in the daytime. This agrees with the result of previous studies showing that the synergistic effect is pronounced in the nighttime and relatively weak in the daytime (Li et al., 2015; Park et al., 2023).

3.2. Interactions of urban heat islands with dry and moist heat waves

In this subsection, we will demonstrate that the interactions between UHIs and DHW are contrasted with those between UHIs and MHW. Fig. 4 presents the composite fields of 200- and 500-hPa geopotential height anomalies and 850-hPa specific humidity anomalies, along with their respective horizontal wind vector anomalies under DHW and MHW. Here, the anomaly is the deviation from the climatological mean over 2001–2022 for July and August. Under DHW, at the 200-hPa level, the structure of the Tibetan high resembles that in the climatological mean (Fig. 4a), while at the 500-hPa level, a retreat of the WNPSH relative to the climatological mean is evident (Fig. 4c). Nonetheless, the anticyclonic circulation anomalies which are elongated in the east-west direction appear over the Korean Peninsula at both levels. This could be to some extent associated with the wave-train from the Scandinavian Peninsula to East Asia in the upper troposphere (partly shown in Fig. 4a, Choi et al., 2020), which needs further investigation. Moreover, at the 500-hPa level, the prominent positive geopotential height anomalies appear on the east of the Kamchatka Peninsula, which may act as a blocking high (Fig. 4c). The Kamchatka blocking high interrupts the eastward movement of the anomalous high-pressure system over the Korean Peninsula and leads to its persistence there, resulting in the occurrence of heat waves (Kim et al., 2018; Yeh et al., 2018; Yoon et al., 2021). The anticyclonic circulation anomalies over the Korean Peninsula act to inhibit the moisture transport from the western North Pacific region (Fig. 4e), contributing to a relatively dry condition over the peninsula. Under MHW, on the other hand, the Tibetan high expands toward the Korean Peninsula (Fig. 4b), and the WNPSH further expands toward the peninsula compared with the climatological mean (Fig. 4d). The expansions of the Tibetan high and WNPSH are known as the dominant causes of heat waves in South Korea (Lee et al., 2020). Furthermore, the moisture transport along the periphery of the expanded WNPSH leads to a relatively moist condition over the Korean Peninsula (Fig. 4f).

The abovementioned differences in large-scale circulation patterns between DHW and MHW are associated with differences in meteorological conditions, soil water, and UHI intensity between DHW and MHW (Table 1). $UHII_{Tmin}$ is 2.57 °C under DHW and 1.27 °C under MHW. $UHII_{Tmax}$ is 0.46 °C under DHW and 0.17 °C under MHW. The difference in $UHII_{Tmin}$ is statistically significant, but the difference in $UHII_{Tmax}$ is statistically insignificant. Interestingly, although both DHW and MHW belong to HW, the daily maximum 2-m temperature under DHW (35.7 °C) is higher than that under MHW (34.3 °C). Relatively higher 10-m wind speed under DHW than under MHW is revealed. The relative humidity is lower under DHW than under MHW according to the DHW and MHW classification. The cloud fraction and volumetric soil water are lower under DHW than under MHW. The lower relative humidity under DHW is associated with the lower cloud fraction and volumetric soil water.

Fig. 5a shows the diurnal variations of differences in urban/rural 2-m temperature between DHW/MHW and nonHW. These differences represent the increases in 2-m temperature in the urban and rural areas due to DHW and MHW in comparison with 2-m temperatures under nonHW. In addition, their distinctions between the urban and rural areas represent the UHI-heat wave interactions under DHW and MHW. In the daytime, in both urban and rural areas, the 2-m temperature difference is much larger under DHW than under MHW. This is consistent with the higher T_{max} under DHW than under MHW (Table 1) and is to some extent associated

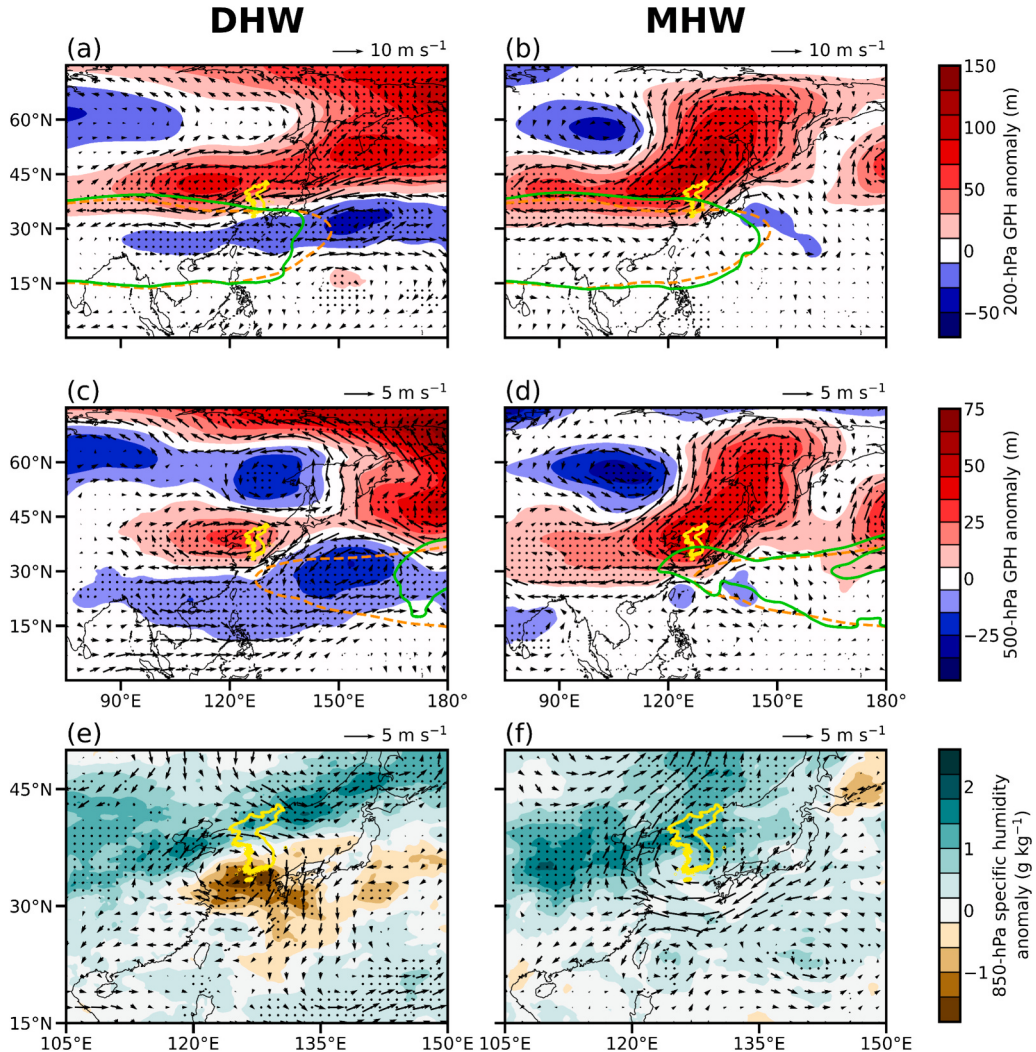


Fig. 4. Composite fields of geopotential height anomalies (shaded) at the (a, b) 200-hPa level and (c, d) 500-hPa level, and (e, f) specific humidity anomalies (shaded) at the 850-hPa level and their respective horizontal wind vector anomalies under (a, c, e) DHW and (b, d, f) MHW. The green contour lines in (a, b) and (c, d) indicate the boundaries of the Tibetan high and WNPSH, respectively. The climatological locations of the boundaries of the Tibetan high and WNPSH are indicated by the orange dashed lines in (a, b) and (c, d), respectively. The yellow solid line denotes the border of the Korean Peninsula. The dotted areas indicate that the anomaly is statistically significant at the 95% confidence level. (For interpretation of the references to colour in this figure legend, the reader is referred to the web version of this article.)

Table 1

Mean UHII_{Tmin}, UHII_{Tmax}, daily maximum 2-m temperature, 10-m wind speed, relative humidity, cloud fraction, and volumetric soil water under DHW and MHW, and their respective differences. The asterisk indicates the statistical significance at the 95% confidence level.

	DHW	MHW	DHW – MHW
UHII _{Tmin} (°C)	2.57	1.27	1.30*
UHII _{Tmax} (°C)	0.46	0.17	0.29
T _{max} (°C)	35.7	34.3	1.4*
10-m wind speed (m s ⁻¹)	1.73	1.45	0.28*
Relative humidity (%)	56.4	75.7	-19.3*
Cloud fraction (1/10)	2.97	5.31	-2.34*
Volumetric soil water (m ³ m ⁻³)	0.22	0.32	-0.11*

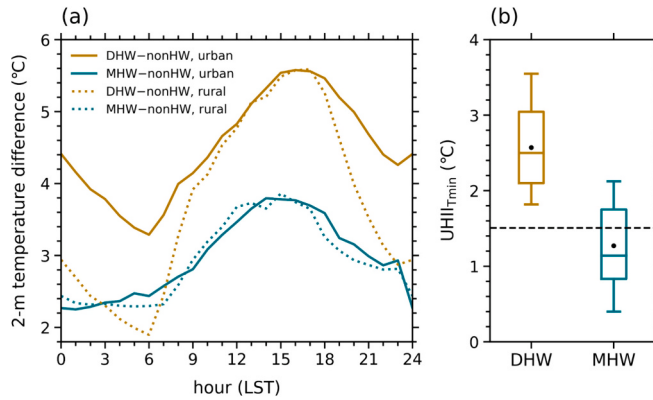


Fig. 5. (a) Diurnal variations of differences in urban/rural 2-m temperature between DHW/MHW and nonHW. The four diurnal variations are DHW minus nonHW in the urban area (darkgold solid line), MHW minus nonHW in the urban area (darkcyan solid line), DHW minus nonHW in the rural area (dotted darkgold line), and MHW minus nonHW in the rural area (dotted darkcyan line). (b) Box plots of $\text{UHII}_{\text{Tmin}}$ under DHW and MHW. The 75th and 25th percentiles are denoted by the upper and lower edges of each box, respectively. The mean and median are denoted by the black dot and horizontal line in each box, respectively. The 90th and 10th percentiles are denoted by the whiskers above and below each box, respectively. The black horizontal dashed line indicates the mean $\text{UHII}_{\text{Tmin}}$ under nonHW.

with relatively clear weather under DHW which is favorable for surface heating by incoming solar radiation. It is seen that under both DHW and MHW, the daytime 2-m temperature differences in the urban and rural areas are similar to each other. This indicates insignificant UHI-heat wave interactions in the daytime. During 18–00 LST, in both urban and rural areas, the 2-m temperature difference decreases under both DHW and MHW. Interestingly, under DHW, the decrease in 2-m temperature difference during 18–00 LST is much larger in the rural area than in the urban area. This results in a larger 2-m temperature difference in the urban area than in the rural area by 1.46 °C during 01–05 LST, which is indicative of prominent nighttime synergistic UHI-heat wave interactions under DHW. On the other hand, under MHW, the urban and rural areas experience similar decreases in 2-m temperature difference during 18–00 LST. This results in similar nighttime 2-m temperature differences between these areas, indicating no significant nighttime UHI-heat wave interactions.

Fig. 5b shows the box plots of $\text{UHII}_{\text{Tmin}}$ under DHW and MHW. Also, the mean $\text{UHII}_{\text{Tmin}}$ under nonHW is shown. Compared to the mean $\text{UHII}_{\text{Tmin}}$ under nonHW, DHW exhibits a distinct increase in mean $\text{UHII}_{\text{Tmin}}$ (1.07 °C). This value is 2.7 times larger than the mean value under HW (0.40 °C), demonstrating a strong synergistic effect. The 10th percentile value of $\text{UHII}_{\text{Tmin}}$ under DHW is also larger than the mean $\text{UHII}_{\text{Tmin}}$ under nonHW. This indicates that most DHW days are exposed to synergistic interactions in the nighttime. In contrast, MHW exhibits a slight decrease in mean $\text{UHII}_{\text{Tmin}}$ (−0.24 °C) compared with the mean $\text{UHII}_{\text{Tmin}}$ under nonHW, with a statistically insignificant difference. This indicates weak negative UHI-heat wave interactions under MHW. The mean and median $\text{UHII}_{\text{Tmin}}$ under MHW are smaller, but its 75th percentile value is larger than the mean $\text{UHII}_{\text{Tmin}}$ under nonHW.

The nighttime UHI arises from more rapid cooling in rural areas than in urban areas. Typically, rural areas exhibit relatively prominent nighttime radiative cooling due to large sky view factors. In contrast, in urban areas, the trapping of longwave radiation, the release of heat stored in the urban canopy, and/or anthropogenic heat impede the nighttime cooling (Oke, 1982). The weather conditions with high relative humidity and cloud fraction hinder the nighttime radiative cooling more effectively in rural areas than in urban areas (Scott et al., 2018) and therefore decrease the urban-rural difference in nighttime cooling. Furthermore, the wet soil conditions weaken the nighttime UHI by increasing thermal admittance of soil more effectively in rural areas than in urban areas (Runnalls and Oke, 2000). As shown in Fig. 5a, the nighttime cooling in the rural area is considerably enhanced under DHW (by 2.33 °C during 18–00 LST) compared to that under nonHW while it is slightly enhanced under MHW (by 0.83 °C). Meanwhile, the nighttime cooling in the urban area is similarly enhanced under DHW and under MHW compared to that under nonHW (by 1.05 °C and 1.32 °C during 18–00 LST, respectively). Thus, the contrasting UHI-heat wave interactions between DHW and MHW appear to be largely due to the different weather and soil water conditions (Table 1) that mainly control rural nighttime cooling.

To assess the importance of relative humidity among weather and soil conditions in determining nighttime UHI-heat wave interactions, a multiple linear regression analysis is performed. The relative humidity, 10-m wind speed, cloud fraction, and volumetric soil water averaged over 01–05 LST and T_{max} in the previous day are used as the predictors of $\text{UHII}_{\text{Tmin}}$ under HW, where all the predictors and $\text{UHII}_{\text{Tmin}}$ are standardized. The 33% of the variance of $\text{UHII}_{\text{Tmin}}$ under HW is explained by the regression model, and the regression coefficients of all predictors except the volumetric soil water and previous-day T_{max} are statistically significant at the 95% confidence level. Among the five predictors, the relative humidity exhibits the largest magnitude of regression coefficient (−0.49), and it is much larger than those for 10-m wind speed (−0.23), cloud fraction (−0.23), volumetric soil water (−0.11), and previous-day T_{max} (0.06). This result indicates that relative humidity under heat waves is the most important meteorological determinant of nighttime UHI-heat wave interactions and is responsible for the above-shown contrasts in the interactions.

Interestingly, the extent to which the mean nighttime UHI-heat wave interaction varies between DHW and MHW (by 1.30 °C) within Daegu appears to be comparable to or even larger than that arising from different background climates or geographical locations. For example, Zhao et al. (2018) revealed that the mean nighttime synergistic UHI-heat wave interaction varies with the city's

background climate from 0.4 °C for U.S. cities with dry climate to 0.7 °C for U.S. cities with continental climate. Jiang et al. (2019) showed that in Beijing (inland) and Shanghai (coastal), China, there is about a 0.6 °C difference in mean nighttime UHI-heat wave interactions. Hence, the above results underline that the variation of UHI-heat wave interaction within a city depending on the humidity of heat waves needs to be thoroughly examined in order to better understand the impacts of UHI-heat wave interactions on urban thermal environment.

3.3. Urban heat stress under dry and moist heat waves

To examine whether the synergistic effect shown in the previous subsection causes the increase in urban heat stress, the four thermal discomfort indices defined in Section 2 are calculated in the urban area during 12–16 LST and 01–05 LST under DHW and MHW (Fig. 6). During 12–16 LST, all the thermal discomfort indices except the discomfort index exhibit statistically significantly larger mean values under MHW than under DHW (Fig. 6a–d). Although DHW exhibits higher temperature than MHW (Fig. 5a), the prominently larger amount of moisture under MHW leads to greater thermal discomfort under MHW. The greater heat stress under MHW than under DHW has been reported in various regions around the world (e.g., Ha et al., 2022; Wouters et al., 2022). During 01–05 LST, on the other hand, the wet-bulb temperature is the only thermal discomfort index that shows significantly larger mean value under MHW than under DHW (Fig. 6h). The Humidex and discomfort index do not show statistically significant differences between DHW and MHW (Fig. 6e and f), and notably, the heat index shows significantly larger mean value under DHW than under MHW (Fig. 6g). Note that this does not happen in the rural area, where all the four indices exhibit larger mean values under MHW than under DHW (not shown). In the urban area, prominent synergistic UHI-heat wave interactions under DHW in the nighttime (Fig. 5a) aggravate heat stress. Given the reduced contribution of relative humidity to thermal discomfort at relatively low temperatures in the nighttime, which is confirmed by evaluating partial derivatives of the indices with respect to relative humidity at different temperature regimes (not shown), the increased urban heat stress by the synergistic UHI-heat wave interactions under DHW counteracts the effect of lower relative humidity and can make DHW as thermally uncomfortable as or even more uncomfortable than MHW. Ha et al. (2022) examined DHW and MHW over a vast area of East Asia and showed that the heat index values under MHW are notably larger than those under DHW. This agrees with our results in the rural area, but not in the urban area in the nighttime. As relatively humid conditions are unfavorable for synergistic UHI-heat wave interactions, the role of humidity in heat stress can be reversed in the urban area in the nighttime, resulting in larger nighttime heat index values under DHW than under MHW.

As shown in Fig. 6e–h, in the nighttime, which of DHW and MHW is more thermally uncomfortable depends on which thermal discomfort index is used. This is because the sensitivities of the four thermal discomfort indices to humidity in high temperature regime

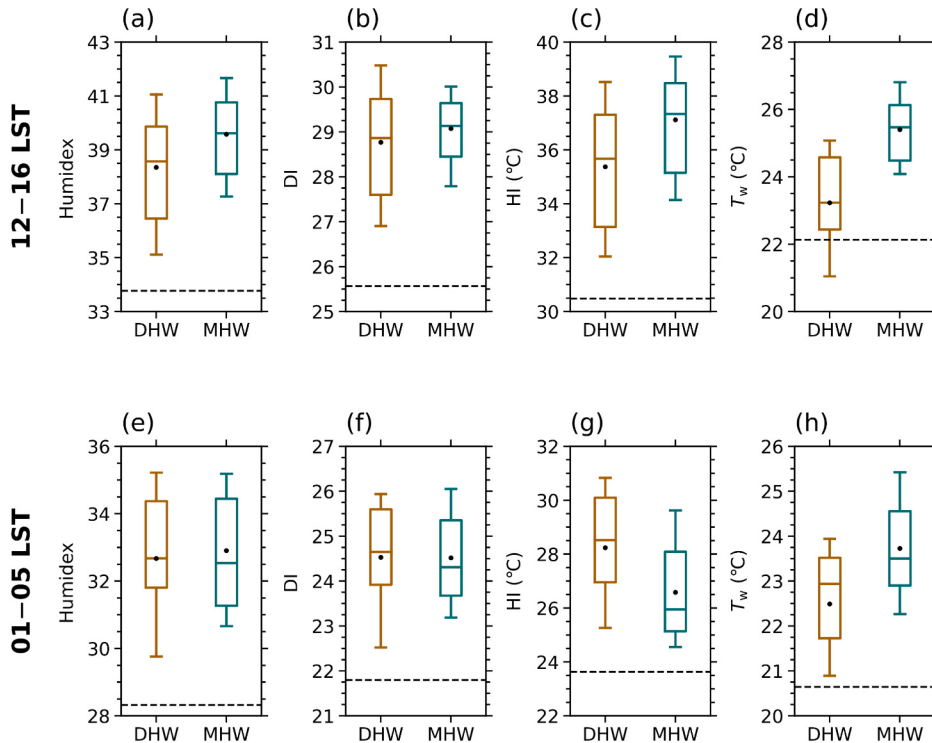


Fig. 6. Box plots of four thermal discomfort indices in the urban area averaged over (a–d) 12–16 LST and (e–h) 01–05 LST under DHW and MHW: (a, d) Humidex, (b, f) discomfort index (DI), (c, g) heat index (HI), and (d, h) wet-bulb temperature (T_w). The meanings of the upper and lower edges of each box, the black dot and horizontal line in each box, and the whiskers above and below each box are the same as those in Fig. 5b.

are different from each other. Based on Eqs. (1)–(4), the partial derivative of each thermal discomfort index with respect to relative humidity is calculated at the HW-mean values of 2-m temperature and relative humidity during 01–05 LST (26.2 °C and 79.8%, respectively), and then it is divided by the HW-mean value of the index. The wet-bulb temperature has the largest sensitivity to relative humidity ($0.0060\%^{-1}$), followed by Humidex ($0.0057\%^{-1}$), discomfort index ($0.0028\%^{-1}$), and heat index ($0.0009\%^{-1}$). This explains the inconsistent results shown in Fig. 6e–h. The differing sensitivities to relative humidity with the thermal discomfort indices may be attributed to the fact that different assumptions (e.g., whether and how human physiology is considered) are adopted in formulating each index (Steadman, 1979; Oleson et al., 2015; Sherwood, 2018; Lu and Romps, 2023).

4. Summary and conclusion

The interactions between urban heat islands in Daegu, South Korea, and dry and moist heat waves are examined using observational and reanalysis data for 2001–2022. Unlike previous studies showing either synergistic or negative UHI-heat wave interactions for a city without classifying types of heat waves, this study demonstrates that the UHI-heat wave interaction can appear in both directions depending on distinct types of heat waves. Different large-scale patterns of heat waves lead to different meteorological conditions in Daegu, and these conditions determine whether the UHI intensity of Daegu will be amplified under heat waves. Under heat waves with high relative humidity (MHW), the nighttime UHI intensity slightly decreases compared to non-heat waves, whereas under heat waves with low relative humidity (DHW), it statistically significantly increases. This highlights the crucial roles of moisture in UHI-heat wave interactions.

Previous studies have reported that the heat stress is greater under MHW than under DHW in various regions around the world (e.g., Ha et al., 2022; Wouters et al., 2022). On the other hand, this study shows that urban residents could experience similar or even greater nighttime heat stress under DHW compared to that under MHW due to the prominent synergistic UHI-heat wave interactions. This emphasizes the necessity of considering UHI-heat wave interactions in assessing and monitoring extreme urban heat stress and also the necessity of UHI mitigation strategies to effectively reduce urban heat-related risks under heat waves.

To get more insights into UHI-heat wave interactions under distinct types of heat waves, observational studies for many cities of the world that belong to different climate zones are needed. In addition, numerical modeling studies are needed to understand mechanisms behind different UHI-heat wave interactions under distinct types of heat waves.

CRediT authorship contribution statement

Dong-Hwi Kim: Writing – review & editing, Writing – original draft, Visualization, Validation, Methodology, Investigation, Formal analysis, Data curation. **Kyeongjoo Park:** Writing – review & editing, Writing – original draft, Methodology, Formal analysis. **Jong-Jin Baik:** Writing – review & editing, Writing – original draft, Supervision, Methodology, Conceptualization. **Han-Gyul Jin:** Writing – review & editing, Methodology, Formal analysis. **Beom-Soon Han:** Writing – review & editing, Formal analysis.

Declaration of competing interest

The authors declare that they have no known competing financial interests or personal relationships that could have appeared to influence the work reported in this paper.

Data availability

Data will be made available on request.

Acknowledgements

The authors are grateful to anonymous reviewers who provided valuable comments on this work. This work was supported by the National Research Foundation of Korea (NRF) under grant 2021R1A2C1007044. Han-Gyul Jin was supported by Global - Learning & Academic research institution for Master's-PhD students, and Postdocs (LAMP) Program of the National Research Foundation of Korea (NRF) grant funded by the Ministry of Education (No. RS-2023-00301938).

References

- An, N., Zuo, Z., 2021. Investigating the influence of synoptic circulation patterns on regional dry and moist heat waves in North China. *Clim. Dyn.* 57, 1227–1240.
- An, N., Dou, J., González-Cruz, J.E., Bornstein, R.D., Miao, S., Li, L., 2020. An observational case study of synergies between an intense heat wave and the urban heat island in Beijing. *J. Appl. Meteorol. Climatol.* 59, 605–620.
- Baik, J.-J., Lim, H., Han, B.-S., Jin, H.-G., 2022. Cool-roof effects on thermal and wind environments during heat waves: a case modeling study in Seoul, South Korea. *Urban Clim.* 41, 101044.
- Blazejczyk, K., Epstein, Y., Jendritzky, G., Staiger, H., Tinz, B., 2012. Comparison of UTCI to selected thermal indices. *Int. J. Biometeorol.* 56, 515–535.
- Chen, X., Li, N., Liu, J., Zhang, Z., Liu, Y., 2019. Global heat wave hazard considering humidity effects during the 21st century. *Int. J. Environ. Res. Public Health* 16, 1513.
- Chew, L.W., Liu, X., Li, X.-X., Norford, L.K., 2021. Interaction between heat wave and urban heat island: a case study in a tropical coastal city, Singapore. *Atmos. Res.* 247, 105134.

- Choi, N., Lee, M.-I., Cha, D.-H., Lim, Y.-K., Kim, K.-M., 2020. Decadal changes in the interannual variability of heat waves in East Asia caused by atmospheric teleconnection changes. *J. Clim.* 33, 1505–1522.
- Epstein, Y., Moran, D.S., 2006. Thermal comfort and the heat stress indices. *Ind. Health* 44, 388–398.
- Founda, D., Santamouris, M., 2017. Synergies between Urban Heat Island and Heat Waves in Athens (Greece), during an extremely hot summer (2012). *Sci. Rep.* 7, 10973.
- Founda, D., Pierros, F., Petrakis, M., Zerefos, C., 2015. Interdecadal variations and trends of the Urban Heat Island in Athens (Greece) and its response to heat waves. *Atmos. Res.* 161–162, 1–13.
- Ha, K.-J., Seo, Y.-W., Yeo, J.-H., Timmermann, A., Chung, E.-S., Franzke, C.L.E., Chan, J.C.L., Yeh, S.-W., Ting, M., 2022. Dynamics and characteristics of dry and moist heatwaves over East Asia. *npj Clim. Atmos. Sci.* 5, 49.
- He, B.-J., Wang, J., Liu, H., Ulipiani, G., 2021. Localized synergies between heat waves and urban heat islands: implications on human thermal comfort and urban heat management. *Environ. Res.* 193, 110584.
- Hersbach, H., Bell, B., Berrisford, P., Hirahara, S., Horányi, A., Muñoz-Sabater, J., Nicolas, J., Peubey, C., Radu, R., Schepers, D., Simmons, A., Soci, C., Abdalla, S., Abellán, X., Balsamo, G., Bechtold, P., Biavati, G., Bidlot, J., Bonavita, M., Chiara, G.D., Dahlgren, P., Dee, D., Diamantakis, M., Dragani, R., Flemming, J., Forbes, R., Fuentes, M., Geer, A., Haimberger, L., Healy, S., Hogan, R.J., Hölm, E., Janíková, M., Keeley, S., Laloyaux, P., Lopez, P., Lupu, C., Radnoti, G., de Rosnay, P., Rozum, I., Vamborg, F., Villaume, S., Thépaut, J.-N., 2020. The ERA5 global reanalysis. *Q. J. R. Meteorol. Soc.* 146, 1999–2049.
- Jiang, S., Lee, X., Wang, J., Wang, K., 2019. Amplified urban heat islands during heat wave periods. *J. Geophys. Res. Atmos.* 124, 7797–7812.
- Kim, M.-K., Oh, J.-S., Park, C.-K., Min, S.-K., Boo, K.-O., Kim, J.-H., 2018. Possible impact of the diabatic heating over the Indian subcontinent on heat waves in South Korea. *Int. J. Climatol.* 39, 1166–1180.
- Lee, W.-S., Lee, M.-I., 2016. Interannual variability of heat waves in South Korea and their connection with large-scale atmospheric circulation patterns. *Int. J. Climatol.* 36, 4815–4830.
- Lee, H.-D., Min, K.-H., Bae, J.-H., Cha, D.-H., 2020. Characteristics and comparison of 2016 and 2018 heat wave in Korea. *Atmosphere* 30, 1–15 (in Korean with English abstract).
- Li, D., Bou-Zeid, E., 2013. Synergistic interactions between urban heat islands and heat waves: the impact in cities is larger than the sum of its parts. *J. Appl. Meteorol. Climatol.* 52, 2051–2064.
- Li, D., Sun, T., Liu, M., Yang, L., Wang, L., Gao, Z., 2015. Contrasting responses of urban and rural surface energy budgets to heat waves explain synergies between urban heat islands and heat waves. *Environ. Res. Lett.* 10, 054009.
- Li, L., Wang, L., Feng, T., Tang, J., Huang, J., Cai, Z., 2023. Multi-index analysis of spatiotemporal variations of dry heat waves and humid heat waves in China. *Atmosphere* 14, 1660.
- Lu, Y.-C., Romps, D.M., 2023. Is a wet-bulb temperature of 35 °C the correct threshold for human survivability? *Environ. Res. Lett.* 18, 094021.
- Luo, M., Wu, S., Liu, Z., Lau, N.-C., 2022. Contrasting circulation patterns of dry and humid heatwaves over southern China. *Geophys. Res. Lett.* 49, e2022GL099243.
- Ngarambe, J., Nganyiyimana, J., Kim, I., Santamouris, M., Yun, G.Y., 2020. Synergies between urban heat island and heat waves in Seoul: the role of wind speed and land use characteristics. *PLoS One* 15, e0243571.
- Oke, T.R., 1982. The energetic basis of the urban heat island. *Q. J. R. Meteorol. Soc.* 108, 1–24.
- Oleson, K.W., Monaghan, A., Wilhelmi, O., Barlage, M., Brunsell, N., Feddema, J., Hu, L., Steinhoff, D.F., 2015. Interactions between urbanization, heat stress, and climate change. *Clim. Chang.* 129, 525–541.
- Park, M.-H., Lee, J.-S., Ahn, W.-S., Kim, H.-D., Oh, S.-N., 2013. A study on the thermal characteristics of midsummer in Daegu metropolitan area. *J. Environ. Sci. Int.* 22, 667–677.
- Park, S., Park, H., Im, J., Yoo, C., Rhee, J., Lee, B., Kwon, C., 2019. Delineation of high resolution climate regions over the Korean Peninsula using machine learning approaches. *PLoS One* 14, e0223362.
- Park, K., Jin, H.-G., Baik, J.-J., 2023. Contrasting interactions between urban heat islands and heat waves in Seoul, South Korea, and their associations with synoptic patterns. *Urban Clim.* 49, 101524.
- Rana, R., Kusy, B., Jurdak, R., Wall, J., Hu, W., 2013. Feasibility analysis of using humidex as an indoor thermal comfort predictor. *Energy Build.* 64, 17–25.
- Raymond, C., Singh, D., Horton, R.M., 2017. Spatiotemporal patterns and synopses of extreme wet-bulb temperature in the contiguous United States. *J. Geophys. Res. Atmos.* 122, 13108–13124.
- Richard, Y., Pohl, B., Rega, M., Pergaud, J., Thevenin, T., Emery, J., Dudek, J., Vairet, T., Zito, S., Chateau-Smith, C., 2021. Is Urban Heat Island intensity higher during hot spells and heat waves (Dijon, France, 2014–2019)? *Urban Clim.* 35, 100747.
- Rogers, C.D.W., Gallant, A.J.E., Tapper, N.J., 2019. Is the urban heat island exacerbated during heatwaves in southern Australian cities? *Theor. Appl. Climatol.* 137, 441–457.
- Runnalls, K.E., Oke, T.R., 2000. Dynamics and controls of the near-surface heat island of Vancouver, British Columbia. *Phys. Geogr.* 21, 283–304.
- Scott, A.A., Waugh, D.W., Zaitchik, B.F., 2018. Reduced Urban Heat Island intensity under warmer conditions. *Environ. Res. Lett.* 13, 064003.
- Sherwood, S.C., 2018. How important is humidity in heat stress? *J. Geophys. Res. Atmos.* 123, 11808–11810.
- Son, J.-Y., Lee, J.-T., Anderson, G.B., Bell, M.I., 2012. The impact of heat waves on mortality in seven major cities in Korea. *Environ. Health Perspect.* 120, 566–571.
- Steadman, R.G., 1979. The assessment of sultriness. Part I: a temperature-humidity index based on human physiology and clothing science. *J. Appl. Meteorol.* 18, 861–873.
- Stull, R., 2011. Wet-bulb temperature from relative humidity and air temperature. *J. Appl. Meteorol. Climatol.* 50, 2267–2269.
- Tan, J., Zheng, Y., Tang, X., Guo, C., Li, L., Song, G., Zhen, X., Yuan, D., Kalkstein, A.J., Li, F., Chen, H., 2010. The urban heat island and its impact on heat waves and human health in Shanghai. *Int. J. Biometeorol.* 54, 75–84.
- Wouters, H., Keune, J., Petrova, I.Y., van Heerwaarden, C.C., Teuling, A.J., Pal, J.S., de Arellano, J.V.-G., Miralles, D.G., 2022. Soil drought can mitigate deadly heat stress thanks to a reduction of air humidity. *Sci. Adv.* 8, eabe6653.
- Xu, K., Lu, R., Kim, B.-J., Park, J.-K., Mao, J., Byon, J.-Y., Chen, R., Kim, E.-B., 2019. Large-scale circulation anomalies associated with extreme heat in South Korea and southern-central Japan. *J. Clim.* 32, 2747–2759.
- Yeh, S.-W., Won, Y.-J., Hong, J.-S., Lee, K.-J., Kwon, M., Seo, K.-H., Ham, Y.-G., 2018. The record-breaking heat wave in 2016 over South Korea and its physical mechanism. *Mon. Weather Rev.* 146, 1463–1474.
- Yoon, D., Cha, D.-H., Lee, M.-I., Min, K.-H., Jun, S.-Y., Choi, Y., 2021. Comparison of regional climate model performances for different types of heat waves over South Korea. *J. Clim.* 34, 2157–2174.
- Zhao, L., Oppenheimer, M., Zhu, Q., Baldwin, J.W., Ebi, K.L., Bou-Zeid, E., Guan, K., Liu, X., 2018. Interactions between urban heat islands and heat waves. *Environ. Res. Lett.* 13, 034003.
- Zong, L., Liu, S., Yang, Y., Ren, G., Yu, M., Zhang, Y., Li, Y., 2021. Synergistic influence of local climate zones and wind speeds on the urban heat island and heat waves in the megacity of Beijing, China. *Front. Earth Sci.* 9, 673786.